Spindle architecture constrains karyotype in budding yeast

Authors

Jana Helsen[1,2]*, Md Hashim Reza[3], Ricardo Carvalho[1], Gavin Sherlock[2]*, Gautam Dey[1]*
[1] Cell Biology and Biophysics, European Molecular Biology Laboratory; Heidelberg, 69117, Germany.
[2] Department of Genetics, Stanford University School of Medicine; Stanford, 94305, USA.
[3] Molecular Mycology Laboratory, Molecular Biology and Genetics Unit, Jawaharlal Nehru Centre for Advanced Scientific Research; Bengaluru, 560064, India.

*Corresponding authors. Emails: jana.helsen@embl.de, gsherloc@stanford.edu, gautam.dey@embl.de

Abstract

The eukaryotic cell division machinery must rapidly and reproducibly duplicate and partition the cell's chromosomes in a carefully coordinated process. However, chromosome number varies dramatically between genomes, even on short evolutionary timescales. We sought to understand how the mitotic machinery senses and responds to karyotypic changes by using a series of budding yeast strains in which the native chromosomes have been successively fused. Using a combination of cell biological profiling, genetic engineering, and experimental evolution, we show that chromosome fusions are well tolerated up until a critical point. Cells with fewer than five centromeres lack the necessary number of kinetochore-microtubule attachments needed to counter outward forces in the metaphase spindle, triggering the spindle assembly checkpoint and prolonging metaphase. Our findings demonstrate that spindle architecture is a constraining factor for karyotype evolution.

Main text

Chromosome fission, fusion, and genome duplications are pervasive across the eukaryotic tree of life and can lead to dramatic differences in chromosome number, even between closely related species. A well-known example of rapid karyotype evolution is found in muntjac deers, whose number of chromosomes varies from 2n = 46 in the Chinese muntjac *Muntiacus reevesi* to 2n = 6/7 in the Indian muntjac *Muntiacus muntjak*[1]. The butterfly genus *Polyommatus* contains species with a haploid chromosome number ranging from n = 10 to n = 226[2], and the ancestor of the model budding yeast, *Saccharomyces cerevisiae*, as a product of interspecies hybridization[3], effectively doubled its number of chromosomes from n = 8 to n = 16 overnight. Each of these examples highlights not only a case of dramatic karyotype rearrangement, but also shows that such changes can occur within relatively short evolutionary timeframes. Despite these changes, every chromosome must still be duplicated faithfully and segregated reliably during mitosis. Failure to do so results in aneuploidy, a state in which cells have an abnormal number of chromosomes, which leads to proteotoxic stress[4], and can result in certain birth defects[5] and cancers[6]. To allow for rapid karyotype evolution, the mitotic machinery must therefore be sufficiently robust to be able to support different genome configurations. Indeed, it is possible to fuse the sixteen native chromosomes of the budding yeast *S. cerevisiae* into one single chromosome[7], or split them up into 33 smaller chromosomes[8] without killing the organism. However, it remains unclear whether such dramatic rearrangements still result in a stable interaction with the different structural components of the cell division machinery, and whether this stability affects organismal fitness and the available trajectories for karyotype evolution. In this study, we use a combination of cell biological characterization and experimental evolution to determine the biophysical constraints dictating chromosome number evolution.

Chromosome fusions induce spindle defects in strains with fewer than five chromosomes

To systematically explore how the cell division machinery copes with changes in chromosome number, we used a series of *S. cerevisiae* strains in which the sixteen native chromosomes have been successively fused by concurrent telomere-to-telomere fusions and centromere excisions[7,9]. The resulting strains have chromosome numbers ranging from sixteen all the way down to one, without significant changes in genome size and content (Fig. 1a). While budding yeast has been shown to tolerate these drastic reductions in chromosome number[7,9], we find that such reductions also come at a fitness cost. By carefully measuring the growth rates of each strain in the series, we show that strains with fewer than five chromosomes have a growth defect corresponding to a five- to ten-minute increase in doubling time across experiments (Fig. 1b, Extended Data Fig. 1a, Extended Data Table 1, summary of effect across multiple experiments in Fig. 4f; for reference, budding yeast doubles about every 1.5 hours). Next, we wanted to test whether this growth defect is can be explained by a delay in mitosis. To do so, we measured the distance between spindle pole bodies (SPBs, Spc42-mCherry) over time, from the moment of pole duplication to the end of anaphase (Fig. 1c-d, Extended Data Fig. 1b, Extended Data Table 2). We show that the time from SPB doubling to the end of anaphase is significantly longer in cells with a growth defect (Fig. 1e). Similarly to what we observe on a population level, single cells with three chromosomes take on average eight minutes longer to progress through mitosis. Since anaphase duration is similar across genotypes (Fig. 1d and also later in Fig. 4b), we hypothesize that the mitotic delay is primarily due to a delay in

metaphase. We also note that while the distance between SPBs during metaphase remains relatively stable at around 1 µm in wild-type cells, it steadily increases in strains with fewer chromosomes (Fig. 1d and also later in Fig. 4b). Strains with fewer chromosomes further also exhibit increased spindle curvature (Extended Data Fig. 1c-e, Extended Data Table 3), as well as atypical distortions of the nuclear envelope during mitosis (Extended Data Fig. 1f). Together, these data indicate that the cell division machinery robustly tolerates chromosome fusions up until 1n = 5. However, strains with fewer chromosomes experience mitotic defects.

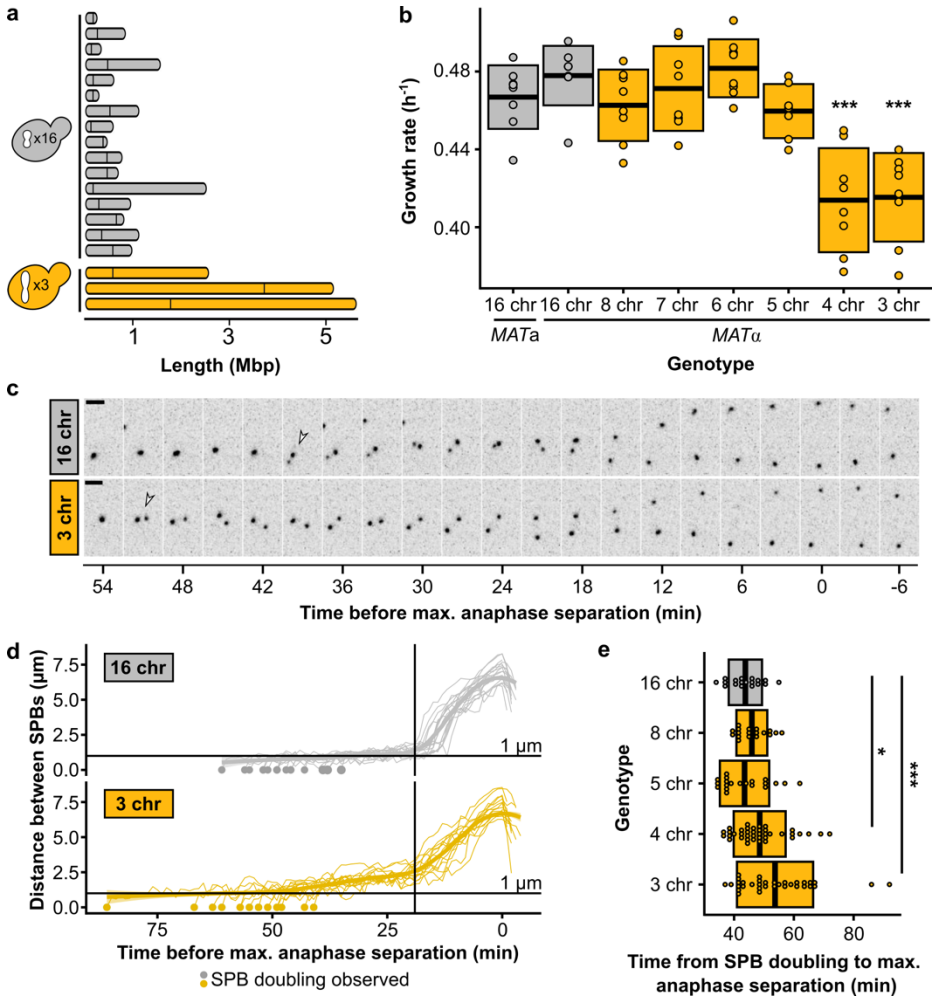

Fig. 1 | Chromosome fusions induce spindle defects from 1n = 4. (a) Chromosome lengths of wild-type (16 chr.) and 3 chr. *Saccharomyces cerevisiae*. Vertical lines indicate positions of centromeres. **(b)** Maximum growth rates of fused-chromosome strains on synthetic complete medium with 2% dextrose (SCD). Boxes show the means and standard deviation. Means were compared to wild type of the same mating type using a Student's t-test; *** $p < 0.001$. **(c)** Montage of SPB (Spc42-mCherry) dynamics during mitosis for 16- and 3-chromosome strains. Scale bar = 2 µm, intervals are 3 minutes. The time point with maximal SPB separation during anaphase was set to zero. Open arrows indicate SPB doubling. **(d)** Distance between SPBs over time. For normalization, the time point with maximal SPB separation during anaphase was set to zero. The vertical line represents the inflection point (~ start of anaphase). **(e)** The time from SPB doubling to max. anaphase separation. Boxes represent the mean and standard deviation. Means were compared using a Student's t-test; * $p < 0.05$, *** $p < 0.001$.

Experimental evolution reveals the growth defect from chromosome fusions can be overcome by diploidization

Next, we sought to determine the molecular mechanisms that underlie the observed growth defect associated with low chromosome numbers. By using experimental evolution, one can evaluate how specific defects can be repaired during evolution, offering insight into what caused the defect in the first place[10]. We established multiple replicate populations of strains with either 16, 8, or 3 chromosomes, and evolved those populations in parallel for ~150 generations (Fig. 2a). We find that evolved strains with three chromosomes were able to completely overcome their initial fitness defect (Fig. 2b, Extended Data Table 4). Remarkably, these evolved strains acquired very few mutations (Fig. 2c), none of which were shared between independently evolved clones (Extended Data Table 5). Additionally, none of the strains evolved by chromosome fission (Fig. 2d, Extended Data Fig. 2). Instead, each and every population that was started from strains with three chromosomes adapted by autodiploidization (Fig. 2e). Diploidization occurs frequently during laboratory evolution, primarily because diploid *S. cerevisiae* cells are known to be more fit than their haploid counterparts in conditions similar to the one we used here[11]. However, the proportion of observed diploids is much higher for evolved 3-chromosome strains compared to evolved 16- or 8-chromosome strains, suggesting that diploidization has a greater fitness benefit in strains with fewer chromosomes. To test if there is positive epistasis between diploidization and low chromosome numbers, we generated isogenic diploids from the ancestral haploid strains and measured their growth rates (Fig. 2f, Extended Data Table 1). Although diploids are more fit overall as expected, the growth defect associated with low chromosome count disappears in 3-chromosome diploids, showing that diploidization is sufficient to completely repair the growth defect.

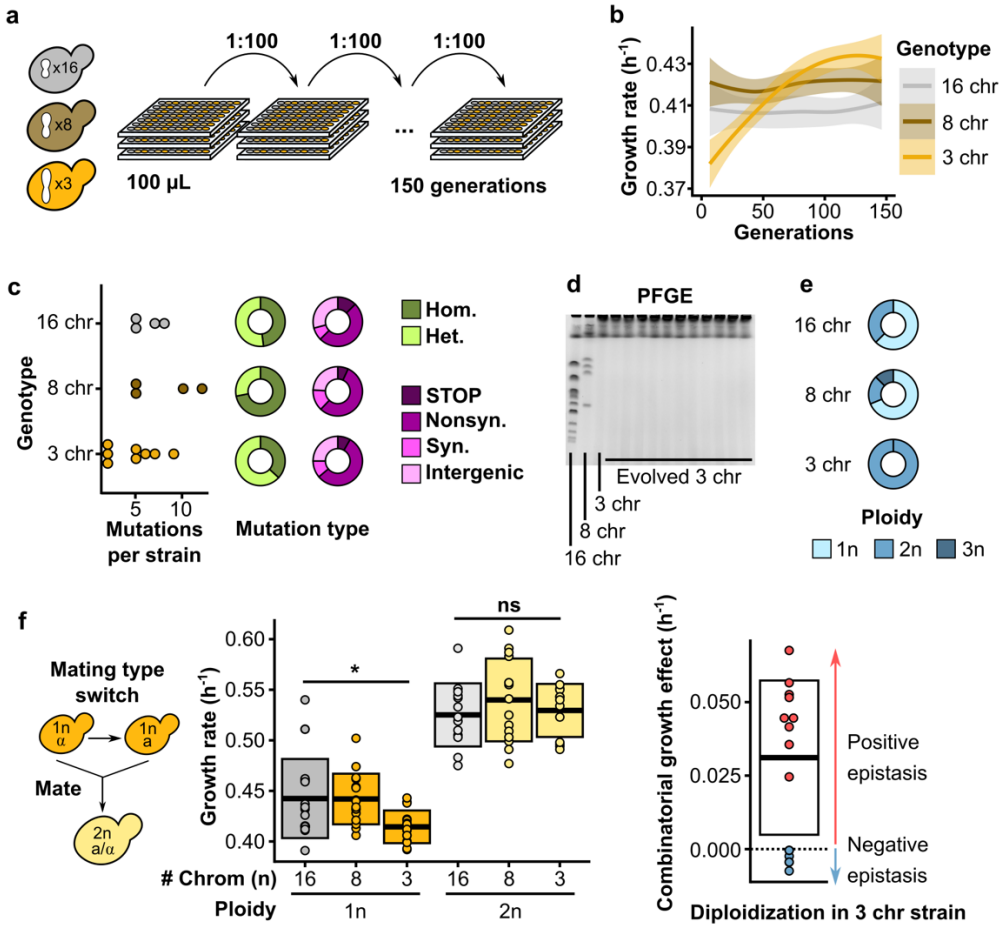

Fig. 2 | Defects are overcome by diploidization during experimental evolution. (a) Schematic overview of the evolution experiments. Replicate populations of strains with either 16, 8, or 3 chromosomes were inoculated in 96-well plates filled with 100 µL SCD, and 1:100 of each culture was transferred daily for a total of ~150 generations. **(b)** Maximum growth rate on SCD over the course of evolution separated by genotype. Curves are smoothed and represent the average trend of 8 replicate evolving populations. Ribbons represent 95% confidence intervals. **(c)** Mutations observed in selected evolved strains. The number of mutations per sequenced strain is shown on the left, the proportions of homozygous and heterozygous mutations are shown in green, and the pink charts show the proportion of nonsense mutations and frameshifts (STOP), nonsynonymous mutations (Nonsyn.), synonymous mutations (Syn.), and intergenic mutations (Intergenic). **(d)** Representative PFGE gel showing the karyotype of the 3 ancestral genotypes and 11 evolved 3-chromosome strains. **(e)** The proportion of ploidies observed in evolved strains separated by genotype. For evolved 16- and 8-chromosome strains, clones from 16 populations were checked for ploidy. For evolved 3-chromosome strains, all 56 populations were checked for ploidy. **(f)** To make diploids, the mating type was switched using a plasmid with inducible HO endonuclease, and cells were allowed to mate to form diploids (left), maximum growth rates of haploid and diploid fused-chromosome strains (middle), and epistasis between chromosome number and ploidy (right). Boxes represent the means and standard deviation. Means were compared using a Student's t-test; * $p < 0.05$.

Five centromeres are sufficient to overcome the mitotic defect

Chromosomes in budding yeasts such as *S. cerevisiae* are each bound by just a single microtubule via its kinetochore[12,13], making it one of the simplest systems in which to study spindle dynamics. From a mitotic perspective, diploidization in this system therefore doubles the number of kinetochore microtubules (kMTs) within the cell. If the mitotic defect is caused by an insufficient number of kMTs or kMT attachments – i.e., fewer than five – diploidization is an easy way for a strain with three chromosomes to increase the number above that threshold. One approach to test this hypothesis is to explore whether the defect can be fixed purely by increasing the total number of centromeres inside the cell. *S. cerevisiae* has a small 'point' centromere of ~120 bp, which can be easily put on a plasmid. Such centromeric plasmids have been shown to interact with the cell division machinery, and the number of kMTs has been shown to be directly proportional to the number of centromeric plasmids inside of a cell[14]. We introduced a centromeric plasmid into a strain with four chromosomes, and found that this indeed fixes both the growth defect (Fig. 3a, Extended Data Table 1) and the mitotic delay (Fig. 3c-d, Extended Data Table 2). In parallel, we transformed a small (9.7 kb) artificial chromosome into the same strains. This chromosome also carries a single centromere, but is more similar to native chromosomes because it is linear and has telomeres. We obtain the same result as for the centromeric plasmid: adding the artificial chromosome rescues the growth defect in the strain with four chromosomes, but not in the strain with three chromosomes (Fig. 3a, Extended Data Table 1). Together, this indicates that rather than the number or size of chromosomes, only the number of centromeres - and hence the number of kMTs and kMT attachments - determines whether a cell experiences a delay. Since adding a centromeric plasmid or artificial chromosome does not alter chromosome size or total chromosomal mass, these observations also preclude the possibility that the size of the fused chromosomes underlies the threshold, i.e., that the chromosomes would have become too large for efficient segregation. Likely, segregation of such large chromosomes is facilitated by increased chromosome condensation during mitosis[15]. This stands in contrast to what is known about mammalian systems, in which chromosome size does seem to affect segregation efficiency[16]. If a budding yeast cell does indeed require more than four centromeres for stable growth, this would suggest that a diploid 2-chromosome strain would still be below that limit and continue to show a growth defect. We diploidized the 2-chromosome strain and measured growth rates and mitotic timing and find that this is indeed the case (Fig. 3b and 3e, Extended Data Fig. 3, Extended Data Table 1 and 2). Together, this shows that having five centromeres, regardless of the number of chromosomes or total DNA content, is sufficient to overcome both the growth and mitotic defect.

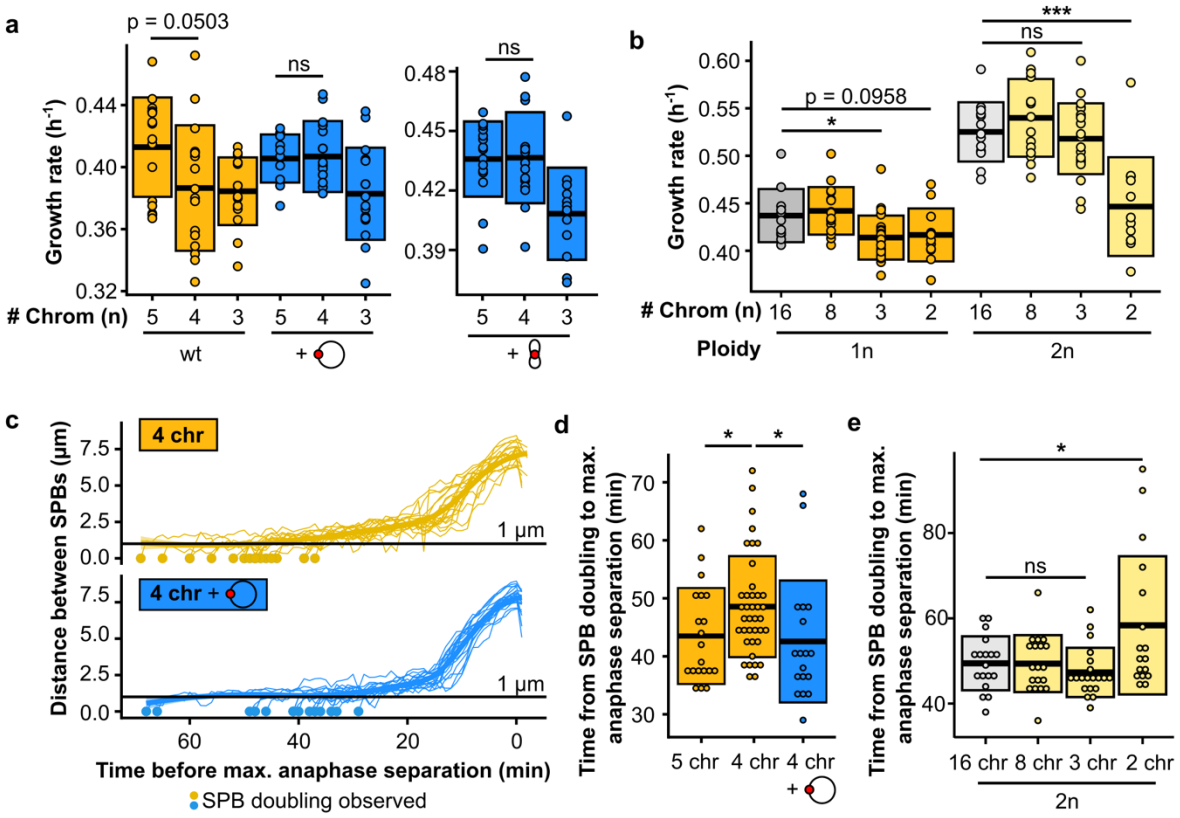

Fig. 3 | Five centromeres are sufficient to overcome the mitotic defect. (a) Maximum growth rates of fused-chromosome strains with and without additional centromere (red circle), supplied on either a plasmid or a small artificial chromosome. Boxes represent means and standard deviation. Means were compared using a Student's t-test. **(b)** Maximum growth rates of haploid and diploid fused-chromosome strains. Boxes represent means and standard deviation. Means were compared using a Student's t-test; * $p < 0.05$, *** $p < 0.001$. **(c)** Distance between SPBs over time for the 4-chromosome strain with and without centromeric plasmid. For normalization, the time point with maximal SPB separation during anaphase was set to zero. **(d)** The time from SPB doubling to max. anaphase separation for the 4-chromosome strain with and without centromeric plasmid. Boxes represent the means and standard deviation. Means were compared using a Student's t-test; * $p < 0.05$. **(e)** The time from SPB doubling to max. anaphase separation for diploid strains. Boxes represent the means and standard deviation. Means were compared using a Student's t-test; * $p < 0.05$.

Decreasing the net outward force in the metaphase spindle alleviates the mitotic defect

kMT attachments are an important contributor to the force balance in metaphase spindles. During metaphase, motor proteins generate an outward force by pushing apart overlapping interpolar microtubules, and cohesion between sister chromatids generates an inward force through kMT attachments (Fig. 4a). Indeed, deleting kinesin-5 motor proteins such as Cin8p or Kip1p shortens the metaphase spindle[14,17], whereas overexpression of Cin8p lengthens it[18]. Additionally, reducing cohesion has been shown to elongate the metaphase spindle[14,19], while increasing the number of kMT attachments shortens it[14]. As noted above, we observe that the distance between SPBs during metaphase increases over time in cells with three chromosomes, much more so than in wild-type cells (Fig. 1d). By characterizing this phenotype in strains with differing numbers of chromosomes, we find that the extent of this

phenomenon negatively correlates with the number of chromosomes (Fig. 4b, Extended Data Fig. 4a, Extended Data Table 2). This suggests that the net outward force in the metaphase spindle increases as the number of kMT attachments decreases, regardless of the total amount of DNA inside the cell. The mitotic defect in strains with fewer than five kMT attachments could therefore be caused by excess outward force during metaphase. Both diploidization as well as the addition of centromeres would fix the defect by increasing the number of kMT attachments and as a result increasing the total amount of inward force. To test this hypothesis, we reduced the amount of outward force by treating the cells with a low concentration of benomyl. Benomyl is a tubulin-binding drug, which at low concentrations can decrease metaphase spindle length by suppressing microtubule dynamics without inducing detachments[20,21]. Treatment with benomyl did indeed fix both the growth and mitotic defect (Fig. 4c-d, Extended Data Fig. 4b, Extended Data Tables 1-2). Additionally, we deleted the motor protein *KIP1* as an orthogonal approach for decreasing the outward force and this too rescued the growth defect (Fig. 4e, Extended Data Table 1). In summary, the growth defect can be completely rescued by either increasing the inward force or decreasing the outward force in the metaphase spindle (Fig. 4f-g, Extended Data Table 2), which implies that an excess of outward force can only be tolerated up until a critical threshold.

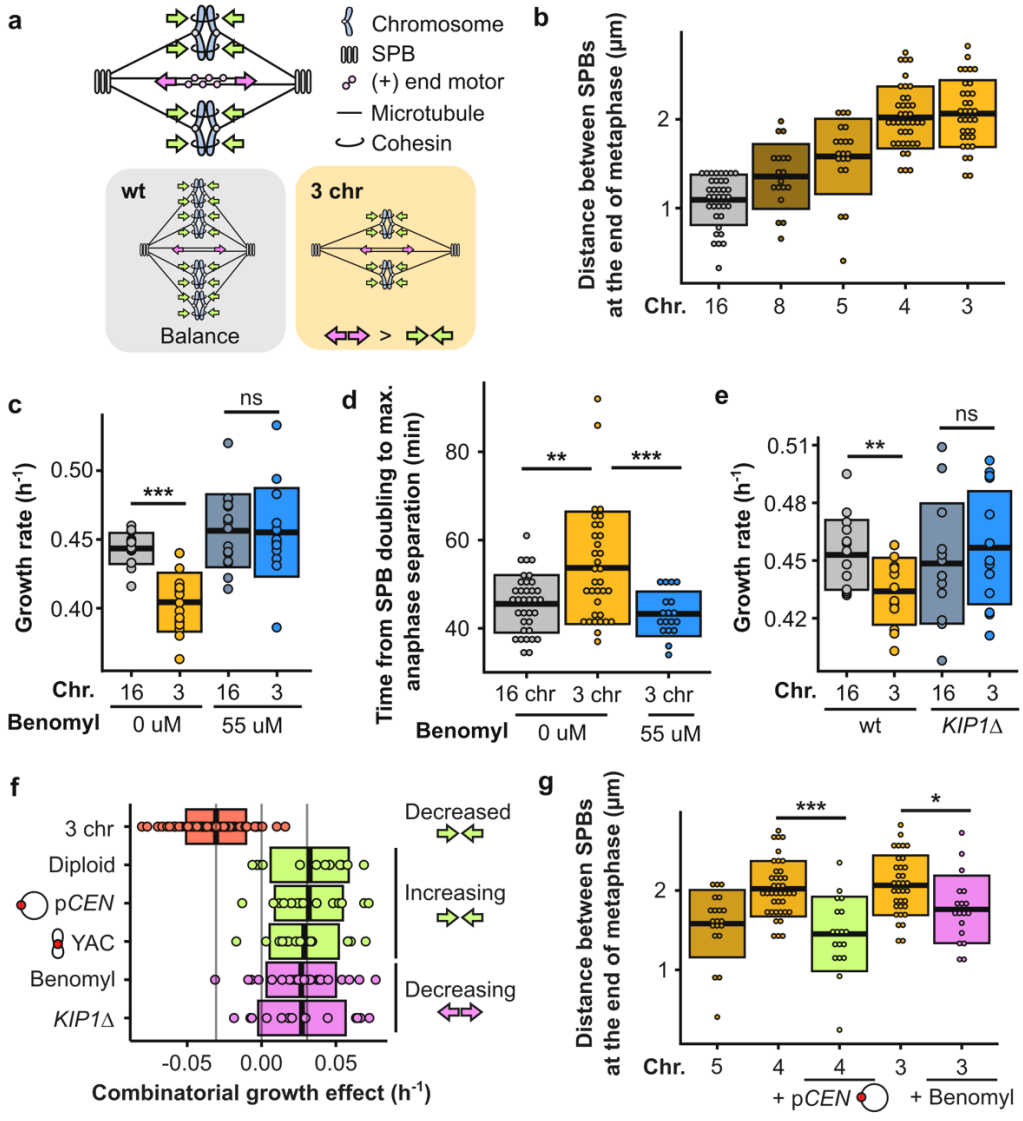

Fig. 4 | Decreasing the net outward force in the mitotic spindle alleviates the defect. (a) Simplified schematic of inward (green arrows) and outward (pink arrows) forces in a metaphase spindle. **(b)** Distance between SPBs at the end of anaphase for different fusion strains. **(c)** Maximum growth rates of fused-chromosome strains with and without benomyl. Boxes represent means and standard deviation. Means were compared using a Student's t-test; *** $p < 0.001$. **(d)** The time from SPB doubling to max. anaphase separation. Boxes represent means and standard deviation. Means were compared using a Student's t-test; ** $p < 0.01$, *** $p < 0.001$. **(e)** Maximum growth rates of fused-chromosome strains with and without *KIP1* deletion. Boxes represent means and standard deviation. Means were compared using a Student's t-test; ** $p < 0.01$. **(f)** Summary of epistatic effects of different perturbations. Diploidization, adding a centromeric plasmid, or adding an artificial chromosome increase the inward force, and adding benomyl or deleting *KIP1* decrease the outward force. Boxes represent means and standard deviation. **(g)** Distance between SPBs at the end of anaphase for different fusion strains and the effects of increasing inward force (+p*CEN*) or decreasing outward force (+benomyl). Means were compared using a Student's t-test; * $p < 0.05$, *** $p < 0.001$.

The force imbalance causes kinetochore declustering and triggers the SAC

As shown in Fig. 4b, the net outward force increases steadily as the number of chromosomes decreases, even in strains without a growth defect or mitotic delay. To explore how this excessive outward force causes an abrupt mitotic defect, we tested whether the spindle assembly checkpoint (SAC) is triggered in these cells. As long as the SAC remains active, transition from metaphase to anaphase is prevented. We deleted *MAD2*, a component of the SAC, which rescued the defect (Fig. 5a-b, Extended Data Fig. 5a,e, Extended Data Tables 1-2), suggesting that activation of the checkpoint underlies the delay in the 3-chromosome strain. Deleting components of other cell cycle checkpoints, such as the DNA damage checkpoint or spindle positioning checkpoint, did not alleviate or exacerbate the defect (Extended Data Fig. 5b-d). For a more direct readout of mitotic timing and SAC activation, we measured Pds1 (securin) levels upon release from a G1 arrest. During metaphase, securin binds and inhibits securase, the protease that degrades cohesin. During the metaphase-to-anaphase transition, securin is degraded, releasing separase so cohesin can be degraded and sister chromatids separated[22]. SAC activation stabilizes Pds1 and therefore prevents this transition, making Pds1 levels a commonly used read-out for SAC activity[23]. Consistent with the five-to-ten-minute delay we observe in the experiments shown above, the 3-chromosome strain displays elevated Pds1 levels at the end of the cell cycle compared to the wild type (+15%), both during the first (Fig. 5d) and second cell cycle (Extended Data Fig. 5f) after G1 release. Together, these observations further support the conclusion that the mitotic delay is more precisely a metaphase delay, in line with our previous experiments. Next, we tested whether there is epistasis between force perturbations and the *MAD2* deletion. If force perturbations and inactivation of the checkpoint fixed the defect by affecting different cellular processes, their effect on growth rate would be additive. Instead, we see negative epistasis (Fig. 5c), indicating that there is a causal link between the force imbalance and the triggering of the SAC.

How does excess outward force in the metaphase spindle lead to SAC activation? During metaphase, sister chromatids must biorient at the center of the mitotic spindle to ensure proper segregation during anaphase. The SAC prevents anaphase initiation until kinetochores from all sister chromatids are correctly attached to kinetochore microtubules from opposite poles. We tagged Ndc80, an outer kinetochore component, to visualize kinetochore dynamics during

metaphase, and observed that kinetochores fail to properly cluster during metaphase in strains with the growth defect (Fig. 5e-f), but reestablish clustering during anaphase. Reducing the amount of outward force by treating the cells with a low concentration of benomyl improves clustering; although the kinetochore foci are still not as defined as in wild-type cells (Fig. 5g), the kinetochore distribution along the spindle during metaphase is restored to a more bilobed (i.e. bimodal) distribution (Fig. 5e, Extended Data Table 6).

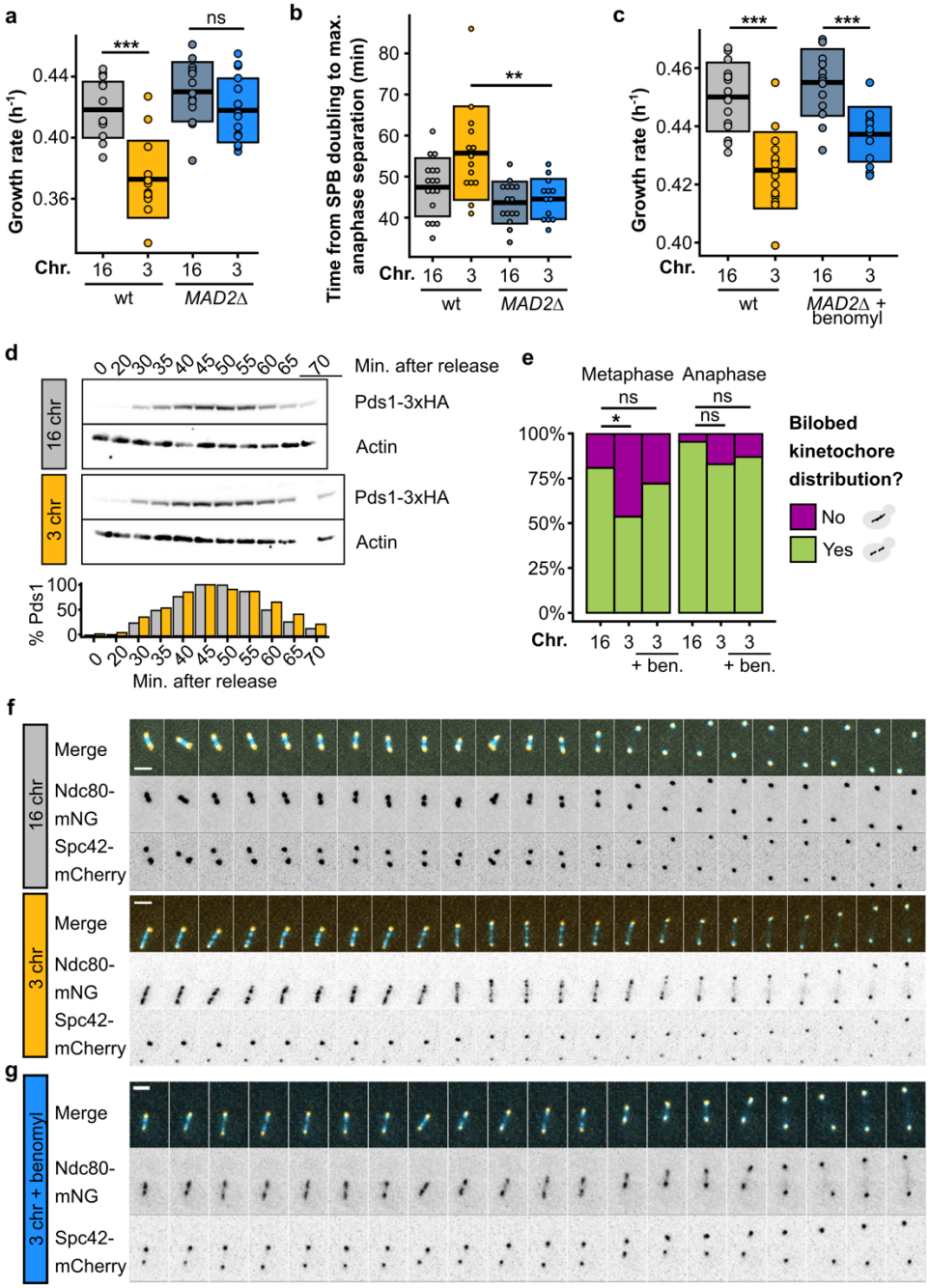

Fig. 5 | The force imbalance causes kinetochore declustering and triggers the SAC. (a) Maximum growth rates of fused-chromosome strains with and without *MAD2* deletion. Boxes represent means and standard deviations. Means were compared using a Student's t-test; *** $p < 0.001$. **(b)** The time from SPB doubling to max. anaphase separation. Boxes represent the means and standard deviations. Means were compared using a Student's t-test; ** $p < 0.01$.

(c) Maximum growth rates of fused-chromosome strains with and without *MAD2* deletion + benomyl treatment (55 µM). Boxes represent means and standard deviations. Means were compared using a Student's t-test; *** $p < 0.001$. **(d)** Western blot analysis of Pds1 levels after G1 release for 16- and 3-chromosome strains. Cells were collected at the indicated time points and alpha factor was added again 45 minutes after release to prevent the cells from entering a second cell cycle. Actin levels were used as a loading control. Pds1-normalised values are shown in the bar plot at the bottom. **(e)** Proportion of cells with a bilobed kinetochore signal (i.e. bimodal Ndc80 signal along the spindle pole to spindle pole axis) in both metaphase and anaphase. Proportions were compared using a two-proportions Z-test; * $p < 0.05$. **(f)** Montage of kinetochore (Ndc80-mNG) and SPB (Spc42-mCherry) dynamics during metaphase for 16- and 3-chromosome strains. Scale bar = 2 µm, intervals are 30 seconds. **(g)** Montage of kinetochore (Ndc80-mNG) and SPB (Spc42-mCherry) dynamics during metaphase in 3-chromosome strains with benomyl (55 µM). Scale bar = 2 µm, intervals are 1 minute.

While further research will be necessary to unravel the exact molecular underpinnings of how excess outward force in the metaphase spindle ultimately leads to activation of the SAC, one hypothesis is that the excess force causes the metaphase spindle to elongate too fast to allow for efficient sister kinetochore pairing, leading to low tension at the kinetochores. Low tension is a signal for improper biorientation, and leads to microtubule detachment through activation of the Aurora B-dependent error correction mechanism[24]. Detached kinetochores in turn trigger the SAC[25]. Alternatively, if the mitotic defect is not caused by tension-dependent detachment, our observations could also be explained by deregulation of kMT length. In *S. cerevisiae*, the length of kMTs has been proposed to control discrimination of bioriented from syntelic attachments during metaphase[26]. In this scenario, declustered kinetochores could still be attached to kMTs, but the kMTs might be too long for efficient detection of biorientation.

Our results show that the spindle architecture of budding yeast robustly supports karyotypes with at least five chromosomes. Below that, cells experience reduced fitness. In nature, the lowest chromosome number observed in other yeast species with similar simple point centromeres is six, in *Kluyveromyces lactis,* a haploid species with a similar genome size to *S. cerevisiae*[27,28]. Budding yeasts have a small spindle with just a single kMT per chromosome, which may exacerbate the effect of low chromosome count on mitosis. Indeed, fission yeast (*Schizosaccharomyces pombe),* which has larger regional centromeres with two to four kMT attachments each[29], has no problem segregating its three native chromosomes. Regardless, budding yeasts are not the only eukaryotes with small spindles. *Ostreococcus tauri*, a species of marine green algae, has a spindle composed of only 10 microtubules[30], and it would be interesting to see if our model can be applied to determine this and other clades' evolutionary limitations on karyotype. Even in species with larger spindles, there is evidence that dramatic karyotypic changes can put evolutionary pressure on components of the cell division machinery. The Indian muntjac *M. muntjak*, whose chromosome number was reduced to 2n = 6/7 through an estimated 26 lineage-specific chromosome fusion events[1], has centromeres that are much larger than those found in its sister species *M. reevesi* (2n = 46)[31]. Remarkably, these large centromeres can bind up to sixty kMTs[32]. Additionally, *M. muntjac*'s genome shows signatures of positive selection in kinetochore proteins CENP-Q and CENP-V[1]. In *Cochlearia*, a plant genus comprising diploid, tetraploid, and hexaploid species, changes in ploidy were shown to correlate with evolution in several kinetochore components, including CENP-E, CENP-C, and INCENP[33]. Our work shows that karyotype and the cell division machinery are

inherently linked during evolution, and it provides insight into how the mechanics of a core cellular process can determine the limitations of evolution.

References

1. Mudd, A. B., Bredeson, J. V., Baum, R., Hockemeyer, D. & Rokhsar, D. S. Analysis of muntjac deer genome and chromatin architecture reveals rapid karyotype evolution. *Commun. Biol.* **3**, 480 (2020).
2. Lukhtanov, V. The blue butterfly *Polyommatus* (*Plebicula*) *atlanticus* (Lepidoptera, Lycaenidae) holds the record of the highest number of chromosomes in the non-polyploid eukaryotic organisms. *Comp. Cytogenet.* **9**, 683–690 (2015).
3. Marcet-Houben, M. & Gabaldón, T. Beyond the Whole-Genome Duplication: Phylogenetic Evidence for an Ancient Interspecies Hybridization in the Baker's Yeast Lineage. *PLOS Biol.* **13**, e1002220 (2015).
4. Oromendia, A. B., Dodgson, S. E. & Amon, A. Aneuploidy causes proteotoxic stress in yeast. *Genes Dev.* **26**, 2696–2708 (2012).
5. Nagaoka, S. I., Hassold, T. J. & Hunt, P. A. Human aneuploidy: mechanisms and new insights into an age-old problem. *Nat. Rev. Genet.* **13**, 493–504 (2012).
6. Ben-David, U. & Amon, A. Context is everything: aneuploidy in cancer. *Nat. Rev. Genet.* **21**, 44–62 (2020).
7. Shao, Y. *et al.* Creating a functional single-chromosome yeast. *Nature* **560**, 331–335 (2018).
8. Ueda, Y. *et al.* Large-scale genome reorganization in *Saccharomyces cerevisiae* through combinatorial loss of mini-chromosomes. *J. Biosci. Bioeng.* **113**, 675–682 (2012).
9. Luo, J., Sun, X., Cormack, B. P. & Boeke, J. D. Karyotype engineering by chromosome fusion leads to reproductive isolation in yeast. *Nature* **560**, 392–396 (2018).
10. Helsen, J., Sherlock, G. & Dey, G. Experimental evolution for cell biology. *Trends Cell Biol.* **33**, 903-912 (2023).
11. Harari, Y., Ram, Y., Rappoport, N., Hadany, L. & Kupiec, M. Spontaneous Changes in Ploidy Are Common in Yeast. *Curr. Biol.* **28**, 825-835.e4 (2018).
12. Winey, M. *et al.* Three-dimensional ultrastructural analysis of the *Saccharomyces cerevisiae* mitotic spindle. *J. Cell Biol.* **129**, 1601–1615 (1995).
13. O'Toole, E. T., Winey, M. & McIntosh, J. R. High-Voltage Electron Tomography of Spindle Pole Bodies and Early Mitotic Spindles in the Yeast *Saccharomyces cerevisiae*. *Mol. Biol. Cell* **10**, 2017–2031 (1999).
14. Nannas, N. J., O'Toole, E. T., Winey, M. & Murray, A. W. Chromosomal attachments set length and microtubule number in the *Saccharomyces cerevisiae* mitotic spindle. *Mol. Biol. Cell* **25**, 4034–4048 (2014).
15. Neurohr, G. *et al.* A Midzone-Based Ruler Adjusts Chromosome Compaction to Anaphase Spindle Length. *Science* **332**, 465–468 (2011).
16. Wang, L.B. *et al.* A sustainable mouse karyotype created by programmed chromosome fusion. *Science* **377**, 967-975 (2022).
17. Straight, A. F., Sedat, J. W. & Murray, A. W. Time-Lapse Microscopy Reveals Unique Roles for Kinesins during Anaphase in Budding Yeast. *J. Cell Biol.* **143**, 687–694 (1998).
18. Saunders, W., Lengyel, V. & Hoyt, M. A. Mitotic spindle function in *Saccharomyces cerevisiae* requires a balance between different types of kinesin-related motors. *Mol. Biol. Cell* **8**, 1025–1033 (1997).
19. Stephens, A. D., Haase, J., Vicci, L., Taylor, R. M. & Bloom, K. Cohesin, condensin, and the intramolecular centromere loop together generate the mitotic chromatin spring. *J. Cell Biol.* **193**, 1167–1180 (2011).

20. Pearson, C. G., Maddox, P. S., Zarzar, T. R., Salmon, E. D. & Bloom, K. Yeast Kinetochores Do Not Stabilize Stu2p-dependent Spindle Microtubule Dynamics. *Mol. Biol. Cell* **14**, 4181–4195 (2003).
21. Edgerton, H. D. *et al.* Low tension recruits the yeast Aurora B protein Ipl1 to centromeres in metaphase. *J. Cell Sci.* **136**, jcs261416 (2023).
22. May, M.M. & Hardwick, K.G. The spindle checkpoint. *J. Cell Sci.* **119**, 4139-4142 (2006).
23. Murillo-Pineda, M., Cabello-Lobato, M.J., Clemente-Ruiz, M., Monje-Casas, F. & Prado, F. Defective histone supply causes condensin-dependent chromatin alterations, SAC activation and chromosome decatenation impairment. *Nucleic Acids Res.* **42**, 12469-12482 (2014).
24. Pinsky, B. A., Kung, C., Shokat, K. M. & Biggins, S. The Ipl1-Aurora protein kinase activates the spindle checkpoint by creating unattached kinetochores. *Nat. Cell Biol.* **8**, 78–83 (2006).
25. Waters, J. C., Chen, R.-H., Murray, A. W. & Salmon, E. D. Localization of Mad2 to Kinetochores Depends on Microtubule Attachment, Not Tension. *J. Cell Biol.* **141**, 1181–1191 (1998).
26. Marco, E. *et al. S. cerevisiae* Chromosomes Biorient via Gradual Resolution of Syntely between S Phase and Anaphase. *Cell* **154**, 1127–1139 (2013).
27. Gordon, J. L., Byrne, K. P. & Wolfe, K. H. Mechanisms of Chromosome Number Evolution in Yeast. *PLoS Genet.* **7**, e1002190 (2011).
28. Friedrich, A. *et al.* Contrasting Genomic Evolution Between Domesticated and Wild *Kluyveromyces lactis* Yeast Populations. *Genome Biol. Evol.* **15**, evad004 (2023).
29. Ding, R., McDonald, K.L. & McIntosh, J.R. Three-dimensional reconstruction and analysis of mitotic spindles from the yeast, Schizosaccharomyces pombe. *J. Cell Biol.* **120**, 141-151 (1993).
30. Gan, L., Ladinsky, M. S. & Jensen, G. J. Organization of the Smallest Eukaryotic Spindle. *Curr. Biol.* **21**, 1578–1583 (2011).
31. Brinkley, B.R., Valdivia, M.M., Tousson, A. & Brenner, S.L. Compound kinetochores of the Indian muntjac. *Chromosoma* **91**, 1-11 (1984).
32. Drpic, D. *et al.* Chromosome segregation is biased by kinetochore size. *Curr. Biol.* **28**, 1344-1356 (2018).
33. Bray, S. M. *et al. Kinetochore and ionomic adaptation to whole genome duplication*. http://biorxiv.org/lookup/doi/10.1101/2023.09.27.559727 (2023) doi:10.1101/2023.09.27.559727.
34. Markus, S. M., Omer, S., Baranowski, K. & Lee, W. Improved Plasmids for Fluorescent Protein Tagging of Microtubules in *Saccharomyces cerevisiae*. *Traffic* **16**, 773–786 (2015).
35. Schwartz, K., Wenger, J. W., Dunn, B. & Sherlock, G. *APJ1* and *GRE3* Homologs Work in Concert to Allow Growth in Xylose in a Natural *Saccharomyces sensu stricto* Hybrid Yeast. *Genetics* **191**, 621–632 (2012).
36. Huxley, C., Green, E. D. & Dunham, I. Rapid assessment of S. cerevisiae mating type by PCR. *Trends Genet.* **6**, 236 (1990).
37. Burke, D.T., Carle, G.F & Olson, M.V. Cloning of large segments of exogenous DNA into yeast by means of artificial chromosome vectors. *Science* **236**, 806-812 (1987).
38. Blazanin, M. *gcplyr: an R package for microbial growth curve data analysis*. http://biorxiv.org/lookup/doi/10.1101/2023.04.30.538883 (2023) doi:10.1101/2023.04.30.538883.
39. Schindelin, J. *et al.* Fiji: an open-source platform for biological-image analysis. *Nat. Methods* **9**, 676–682 (2012).

40. Kryazhimskiy, S., Rice, D. P., Jerison, E. R. & Desai, M. M. Global epistasis makes adaptation predictable despite sequence-level stochasticity. *Science* **344**, 1519–1522 (2014).
41. Li, H. Aligning sequence reads, clone sequences and assembly contigs with BWA-MEM. (2013) doi:10.48550/ARXIV.1303.3997.
42. McKenna, A. *et al.* The Genome Analysis Toolkit: A MapReduce framework for analyzing next-generation DNA sequencing data. *Genome Res.* **20**, 1297–1303 (2010).
43. Thorvaldsdottir, H., Robinson, J. T. & Mesirov, J. P. Integrative Genomics Viewer (IGV): high-performance genomics data visualization and exploration. *Brief. Bioinform.* **14**, 178–192 (2013).
44. Todd, R. T., Braverman, A. L. & Selmecki, A. Flow Cytometry Analysis of Fungal Ploidy. *Curr. Protoc. Microbiol.* **50**, e58 (2018).
45. Hinterndorfer, K. *et al.* Ultrastructure expansion microscopy reveals the cellular architecture of budding and fission yeast. *J. Cell Sci.* **135**, jcs260240 (2022).
46. Gambarotto, D. *et al.* Imaging cellular ultrastructures using expansion microscopy (U-ExM). *Nat. Methods* **16**, 71–74 (2019).
47. Knop M. *et al.* Epitope tagging of yeast genes using a PCR-based strategy: more tags and improved practical routines. *Yeast* **15**, 963-972 (1999).

Acknowledgements

The authors would like to thank Omaya Dudin, Michelle Hays, Buzz Baum, Jordi van Gestel, Lars Steinmetz, Ishier Raote, Felix Mikus and other members of the Dey and Sherlock labs for critical feedback on the manuscript.

Funding

Life Science Alliance Bridging Excellence Fellowship (JH)
EMBL Corporate Partnership Programme Fellowship (HR)
EMBO Scientific Exchange Grant 10212 (HR)
Department of Biotechnology-Research Associate Fellowship (HR)
NIGMS R35 GM131824 (GS)
European Molecular Biology Laboratory (JH, RC and GD)
European Union (ERC, KaryodynEvo, 101078291) (JH and GD)

Author contributions

Conceptualization: JH, GS, GD
Methodology: JH, GS, GD
Investigation: JH, HR, RC, GS, GD
Formal analysis: JH
Visualization: JH
Funding acquisition: JH, GS, GD
Project administration: JH, GS, GD
Supervision: GS, GD
Writing - original draft: JH, HR, GS, GD
Writing - review & editing: JH, HR, GS, GD

Competing interests

Authors declare that they have no competing interests.

Data and materials availability

All images used for data analysis are available at doi.org/10.6084/m9.figshare.c.6890251.v2. Sequencing data were deposited on ENA under accession number PRJEB67700. Raw measurements used for plotting can be found in the supplementary data files.

Methods

Strains

Full genotypes of all strains used in this study can be found in Extended Data Table 7. Strains were constructed using the standard LiAc-based transformation protocol for budding yeast. Proteins were tagged C-terminally with mNeongreen using a mNeonGreen:HphNT1 cassette, with mCherry using a mCherry:NatNT2 cassette, with 3xHA using a 3xHA:HphNT1 cassette and Tub1 was tagged N-terminally using Addgene vector #50654[34]. Genes were deleted using a KanMX4 cassette. Strains were diploidized by mating-type switching and mating in batch, using a plasmid containing HO endonuclease as previously described[35], and ploidy was verified using PI staining (see below). Mating types were confirmed using mating-type specific primers as previously described[36]. Centromere plasmids contained *CEN4, ARS1* and either KanMX4 or HphMX for selection. Cloning vector pYAC4 was used as a small artificial chromosome after linearization[37].

Growth assays

All growth assays were performed on synthetic complete medium with 2% dextrose (SCD). Per genotype, two biological replicates were inoculated in 150 µL SCD and serially diluted for overnight growth at 30°C in a 96-well plate. The next morning, log phase cultures at OD_{600} < 0.1 were selected and 5 µL of each selected culture was inoculated in 95 µL SCD in a 96-well plate. For each strain, this was repeated so that there were eight technical replicates per culture, and 16 replicate measurements per genotype in total. By consecutive culturing, we ensured that every culture is growing exponentially before the start of the growth experiment. The plate was incubated at 30°C with continuous double orbital shaking in a BioTek Epoch2 microplate reader (Agilent), and the OD_{600} was measured every 10 minutes for 24 hours. Maximum growth rates were determined using the gcplyr package in R[38]. For growth assays with benomyl (Sigma) or hydroxyurea (Sigma), all strains were pre-grown on SCD without the chemical compound and the chemical compound was added for the actual growth assay.

Live-cell microscopy

Strains were imaged live in 8-chamber glass bottom dishes (Ibidi) in SCD at 30°C. The dishes were coated with 1 mg/mL Concanavaline A (Sigma), and log phase cells were pipetted into the chambers after which they were allowed to settle for 30 minutes at 30°C. The medium was removed by pipetting, and replaced by fresh SCD after one wash to remove unattached cells. All live-cell microscopy experiments were done using an Olympus IXplore SpinSR spinning disk confocal microscope with CSU-W1 (Yokogawa), 50 µm pinholes, and a Flash4 sCMOS camera (Hamamatsu). Samples were illuminated with 488 nm (mNeonGreen or CloverGFP) and 561 nm (mCherry) lasers. The microscope was controlled by cellSens software (Olympus). SPB time-lapses, spindle time-lapses, spindle snapshots were made using a UPLXAPO 60X oil immersion objective (NA 1.42, Olympus). Kinetochore time-lapses and snapshots were made using a UPLSAPO-S 100X silicone immersion objective (NA 1.35, Olympus). For spindle time-lapses, cells were imaged using 15 z-stacks with a step size of 0.27 µm, for spindle snapshots, 23 z-stacks with a step size of 0.27 µm, for SPB time-lapses, 15 z-stacks with a step size of 0.36 µm, for kinetochore time-lapses, 15 z-stacks with a step size of 0.28 µm, and for kinetochore snapshots, 23 z-stacks with a step size of 0.28 µm.

Image analysis

Fiji[39] was used for basic image processing (cropping, z-stack projections, scaling, LUT selection), and for measuring spindle curvature and SPB distance over time. To measure SPB distance over time, maximum intensity projections were made of 3-hour time-lapses of Spc42-tagged strains, using 1-minute intervals. Per genotype, ~20 ROIs were selected of cells in which SPBs could be followed from the moment of duplication up until collapse of the spindle. The straight line tool was used to measure inter-SPB distance for each timepoint. To quantify spindle curvature, maximum intensity projections were made of snapshot images of Tub1-tagged strains. Within each image, up to 10 ROIs were selected of cells with clear anaphase spindles. For each genotype, 50 ROIs were selected in total (5-6 different images). The straight line tool was used to measure the distance between both ends of the spindle, and the freehand line tool was used to trace the spindle and estimate spindle length. The spindle curvature was defined as the difference between the two measures, divided by the straight distance. To quantify the proportion of cells with bilobed kinetochore distributions, ROIs were selected of dividing cells with a clear Ndc80-mNG and Spc42-mCherry signal (wild type: n = 50, 3-chromosome strain: n = 97, 3-chr + benomyl: n = 131). Using the straight line tool, inter-SPB distance was measured and used to classify cells into metaphase (inter-SPB distance < 1.25 µm for wild type, < 2.5 µm for 3-chromosome strain) or anaphase (inter-SPB distance > 1.25 µm for wild type, > 2.5 µm for 3-chromosome strain). The rotated rectangle tool was used to select an area from SPB to SPB, after which a profile plot was generated to visualize the distribution of the Ndc80 signal. This plot in turn was used to quantify the proportion of cells with a 'bilobed' (i.e., bimodal) signal.

Experimental evolution

For each genotype (16, 8, and 3-chromosome strains), 56 replicate populations were established by inoculating single colonies in different wells of a 96-well plate containing 100 µL SCD. Populations were transferred daily around the same time, by inoculating 1 µL of old culture into 100 µL fresh SCD. Cells were grown at 30°C with shaking. Every population reached saturation after 24 hours, so we used the dilution factor (1:100) to estimate the number of generations per transfer (~6.7). To monitor average growth rate throughout evolution, one of the 96-well plates was evolved in the BioTek Epoch2 microplate reader (Agilent). Populations were frozen every fourth transfer and at timepoints of particular interest (e.g., 100 generations). The experiment was stopped at 150 generations, at which point the growth rate data indicated that 3-chromosome strains had repaired their growth defect. For sequencing and ploidy determination, frozen populations were streaked on YPD plates to isolate single clones. Whole populations were grown for pulsed-field gel electrophoresis.

Whole-genome sequencing

The YeaStar genomic DNA kit (Zymo research) was used to isolate genomic DNA from single clones. Sequencing libraries were prepared using the Nextera kit as previously described[40], starting with 5-10 ng of genomic DNA. The quality of the pooled libraries was assessed by measuring concentrations on the Qubit (Invitrogen) and fragment size distribution on a Bioanalyzer platform (Agilent). Samples were sent for paired-end sequencing on an Illumina HiSeq X, with an average read length of 150 bp. The quality of the reads was assessed using FastQC version 0.11.9 (Babraham Bioinformatics), and Nextera transposase sequences were trimmed using Trim galore! version 0.6.7 (Babraham Bioinformatics). Trimmed reads were mapped to the reference S288c genome (version R64) using bwa-mem version 0.7.17 with

default settings[41]. Indels and SNVs were called using GATK version 4.2.6.1[42], using HaplotypeCaller and default settings. Variants present in the ancestral strains were filtered out, as well as SNVs with a quality score below 175, and indels with a quality score below 200. Finally, all remaining SNVs and indels were verified by manual curation in IGV[43].

Pulsed-field gel electrophoresis

Yeast chromosome plugs were prepared as described in the Bio-Rad CHEF DR-III manual. Briefly, 0.25 mL of stationary overnight culture was washed twice in 10 mL ice-cold 50 mM EDTA. Cells were resuspended in 250 µL cell suspension buffer (10 mM Tris, 50 mM EDTA, 2 mM NaCl), spun down, and resuspended in 40 µL cell suspension buffer. 10 µL lyticase (Sigma) stock (1000 U/mL) was added, and the cell suspension was mixed with 50 µL molten 2% CleanCut agarose (Bio-Rad) after which the mixture was pipetted into a plug mold (Bio-Rad). Plugs were allowed to solidify on ice, and were then pushed out of the molds into microcentrifuge tubes with 0.5 mL lyticase buffer (10 mM Tris, 50 mM EDTA) with 30 µL lyticase stock. The plugs were incubated at 37°C for 2 hours, after which they were transferred to new microcentrifuge tubes with 0.75 mL proteinase K buffer (10 mM Tris, 100 mM EDTA, 0.5% SDS) with proteinase K (23 U/mL). The plugs were incubated at 50°C overnight, after which they were equilibrated in new microcentrifuge tubes with 0.5X TBE before insertion into the gel (½ plug per lane). The gel was made using Pulsed Field Certified Agarose (1%, Bio-Rad) in 0.5X TBE, and was run on a CHEF-DR III Pulsed-Field Gel Electrophoresis System (Bio-Rad), at 6 V/cm, 120°, switch time 60-120 seconds, for 24 hours at 14°C. The gel was stained with GelRed (Sigma) for visualization.

Ploidy determination

Ploidy was determined as described previously by staining the cells with propidium iodide[44]. A haploid (BY4741) and diploid (BY4743) strain were used as controls, and fluorescence of 30,000 cells was analyzed by flow cytometry on an Acea Novocyte Quanteon (Agilent).

Ultrastructure expansion microscopy

Ultrastructure expansion microscopy (U-ExM) was performed as previously described[45,46] with a few modifications. Briefly, log-phase cells were fixed with 4% HCHO (FA) in PEM buffer (100 mM PIPES, 1 mM EGTA, 1 mM $MgSO_4$, pH 9.0), washed twice with 1X PBS and once with PEM-S (1.2 M sorbitol in PEM). The fixed cells were resuspended in PEM-S buffer and were enzymatically digested with 2.5 mg/mL Zymolyase 20T at 37°C with agitation for 15 minutes. Cells were washed once with PEM-S buffer. This was followed by overnight anchoring in acrylamide (AA)/FA (1% AA, 0.7% FA diluted in 1X PBS) at 37°C. The anchored cells were then allowed to attach to a 6 mm Poly-l-lysine coated coverslip for 1 hour. Gelation was performed on ice using a monomer solution (19% (wt/v) sodium acrylate, 10% (v/v) acrylamide, 0.1% (v/v) N, N'- methylenebisacrylamide in PBS) and the gel was kept for polymerization for 1 hour at 37°C in a moist chamber. For denaturation, the gel was transferred to denaturation buffer (50 mM Tris pH 9.0, 200 mM NaCl, 200 mM SDS, pH 9.0) and incubated at 95°C for 1.5 hours. Following denaturation, the gel was expanded with three subsequent washes with water. Post expansion, the gel diameter was measured to determine the expansion factor. For ExM images, scale bars have not been rescaled for the gel expansion factor. Pan-labelling for ExM was done at 1:500 with DyLight™ 594 NHS ester (Thermo Fischer Scientific, 46412) in 1X PBS overnight at 4°C. For tubulin immunostaining, the gel was stained using YL1/2 anti-α-tubulin (rat) (kind gift from Gislene Pereira [COS Heidelberg, Germany]),

as the primary antibody at 1:25 and incubated overnight at 4°C. The gel was then incubated with goat anti-mouse-IgG coupled to Alexa Fluor 488 (Invitrogen A11029) secondary antibody at 1:1000 and incubated at 37°C for 3 hours in the dark. The antibody dilutions were prepared in 3% BSA in 1X PBS with 0.1% Tween 20. The gel was washed thrice with PBS with 0.1% Tween 20 for 30 minutes at room temperature. The gel was expanded with three subsequent washes with water before imaging. For microscopy, Poly-l-lysine coated 2-chamber glass bottom dishes (ibidi) were used. Gels were cut to an appropriate size to fit the ibidi chambers. The gels were overlaid with water to prevent drying or any shrinkage during imaging. The gels were imaged using the Zeiss LSM980 Airyfast confocal microscope using a Plan-Apochromat 63x/1.4 Oil DIC M27 objective.

Western blot for Pds1 dynamics after alpha factor arrest

To be able to arrest the 3-chromosome strain with alpha factor, we switched the strain's mating type from *MAT*α to *MAT*a using the method described above under 'Strains'. Additionally, we endogenously tagged Pds1 with 3xHA in both the wild-type and 3-chromosome strain. Cells were inoculated in 5 mL YPAD in the morning, and this preculture was used to inoculate a 100 mL YPAD overnight culture so that the culture would reach OD_{600} 0.2 the next morning. Cells were grown at 30°C throughout the experiment. The next morning, cells were diluted once more and grown for an additional 1.5 hours, so that we had stable 100 mL log-phase cultures of OD_{600} 0.2 to the start the arrest. The cells were then arrested in G1 using a final concentration of 4.0 µg/mL alpha-factor mating pheromone (Zymo Research) and incubated at 30°C with shaking until the vast majority of cells in the population exhibited the 'shmoo' phenotype (2.5 hours). G1-arrested cells were released by washing them trice in pre-warmed YPAD after which they were grown at 30°C and samples collected as needed. For one of the two experiments we prevented the cells from going into a second cell cycle by adding 4.0 µg/mL alpha-factor mating pheromone 45 minutes after release. For each time point, 2 mL of the culture were pelleted and snap-frozen using liquid nitrogen. The cell pellets were lysed by TCA precipitation[47] and resuspended in 50 µL of High Urea DTT buffer (200 mM Tris-HCl pH 6.8, 8 M urea, 5% w/v SDS, 1 mM EDTA, 100 mM DTT, bromophenol blue). Pds1 levels were monitored using a mouse anti-HA antibody (Cat. No. 26183, Invitrogen, 1:1000 dilution), actin levels were analyzed using a mouse anti-actin antibody (Cat. No. MAB1501R, Chemicon, 1:1000 dilution), and an HRP-conjugated goat anti-mouse secondary antibody (Cat. No. 31430, Invitrogen, 1:10000 dilution). The blots were developed using a chemiluminescence substrate (Millipore Cat. No. WBULP) and imaged using an Azure 280 imaging system (Azure). The Pds1 values shown in the plots were normalized to the timepoint with the highest Pds1 signal (45 minutes for the experiment shown in Fig. 5d, 105 minutes for the experiment shown in Extended Data Fig. 5f).

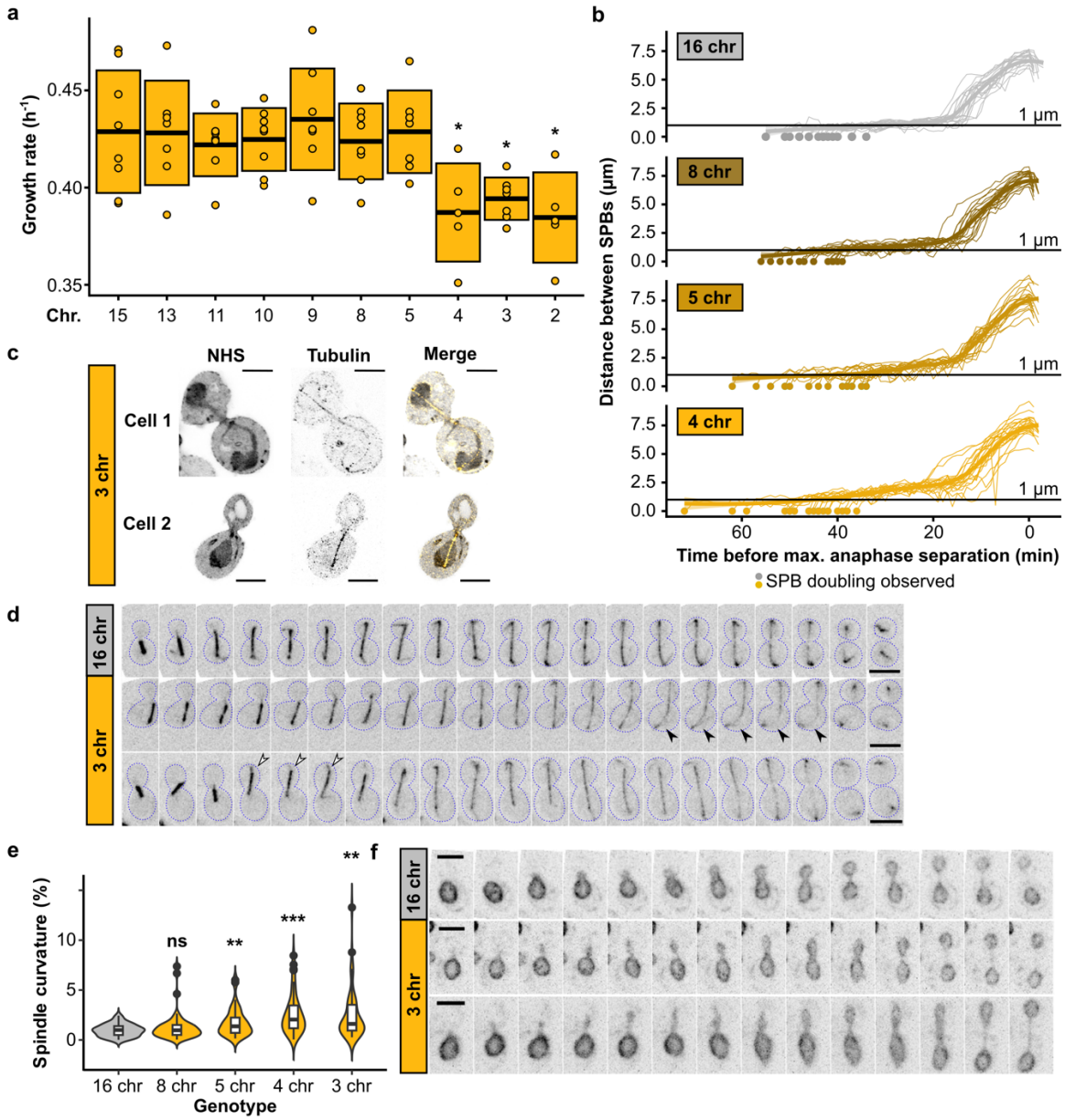

Extended Data Fig. 1 | Growth and mitotic defects in fused-chromosome strains. (a) Maximum growth rates of fused-chromosome strains on synthetic complete medium with 2% dextrose (SCD). Boxes show the means and standard deviation. Means were compared using a Student's t-test; * $p < 0.05$ **(b)** Distance between SPBs over time for different fusion strains. For normalization, the time point with maximal SPB separation during anaphase was set to zero. **(c)** Expanded cells with spindle defects. Cells were labeled with pan protein label NHS ester and for tubulin. Scale bar = 10 µm, expansion factor = 4.18. **(d)** Montage of spindle dynamics over time (CloverGFP-tub1). Scale bar = 5 µm, intervals are 1 min. Closed arrows point to an example of increased spindle curvature, open arrows to an example of the whole spindle moving into the daughter cell. **(e)** Spindle curvature (%), calculated as the total spindle length relative to the distance between spindle pole bodies (SPBs). n = 50 for each genotype. Distributions were compared using Kolmogorov-Smirnov tests; ** $p < 0.01$, *** $p < 0.001$. **(f)** Montage of nuclear envelope (Hmg1-mCherry) dynamics over time. Scale bar = 5 µm, intervals are 1 min.

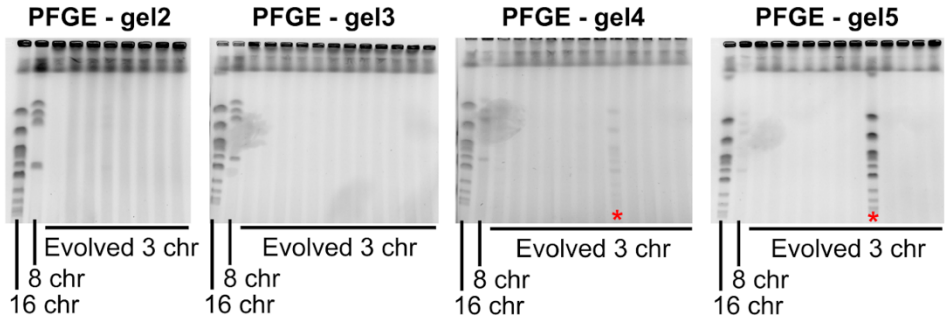

Extended Data Fig. 2 | PFGE of evolved strains shows no chromosome fission. PFGE gels showing the karyotype of the evolved 3-chromosome populations. Red stars indicate populations with cross-contamination of a wild-type strain. Chromosome numbers of clones isolated from these populations were double-checked before ploidy determination and sequencing.

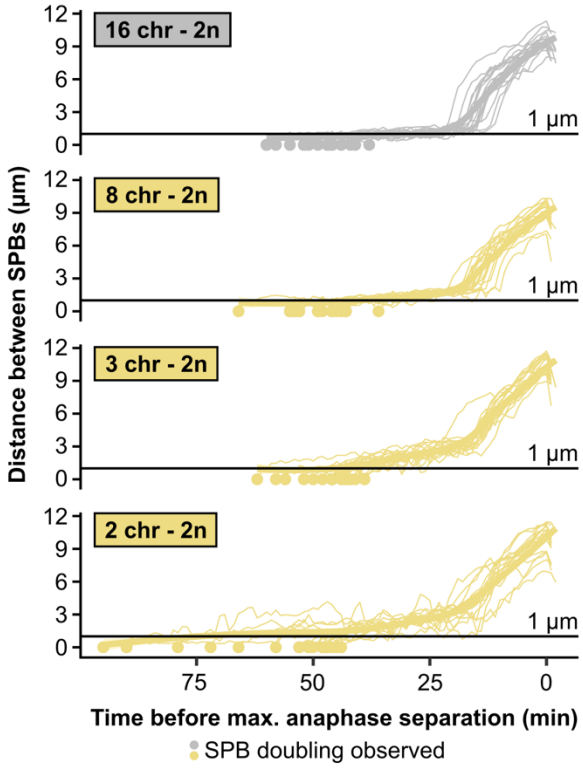

Extended Data Fig. 3 | Distance between SPBs over time in diploids. For normalization, the time point with maximal SPB separation during anaphase was set to zero.

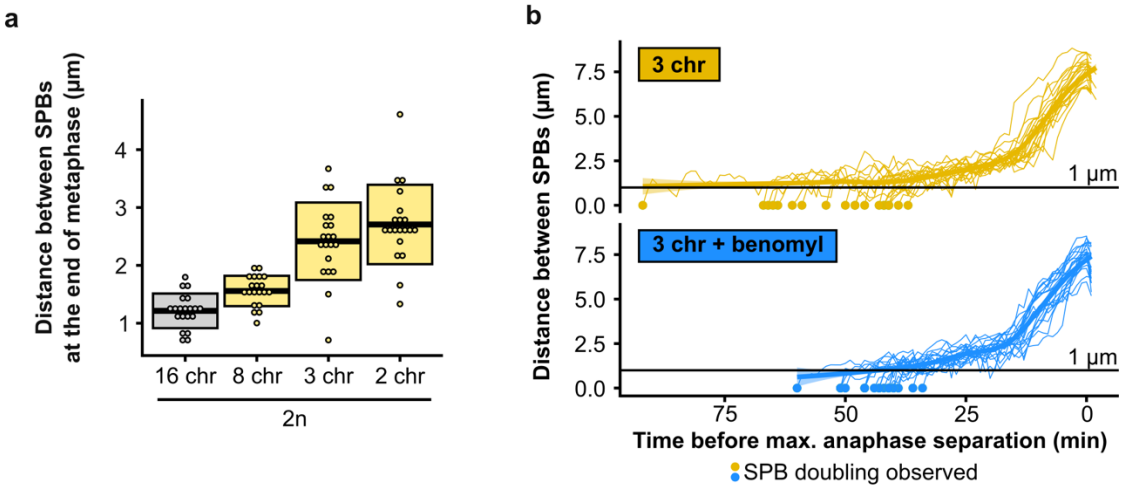

Extended Data Fig. 4 | (a) Distance between SPBs at the end of anaphase for different diploid fusion strains. **(b)** Distance between SPBs over time in benomyl-treated cells. For normalization, the time point with maximal SPB separation during anaphase was set to zero.

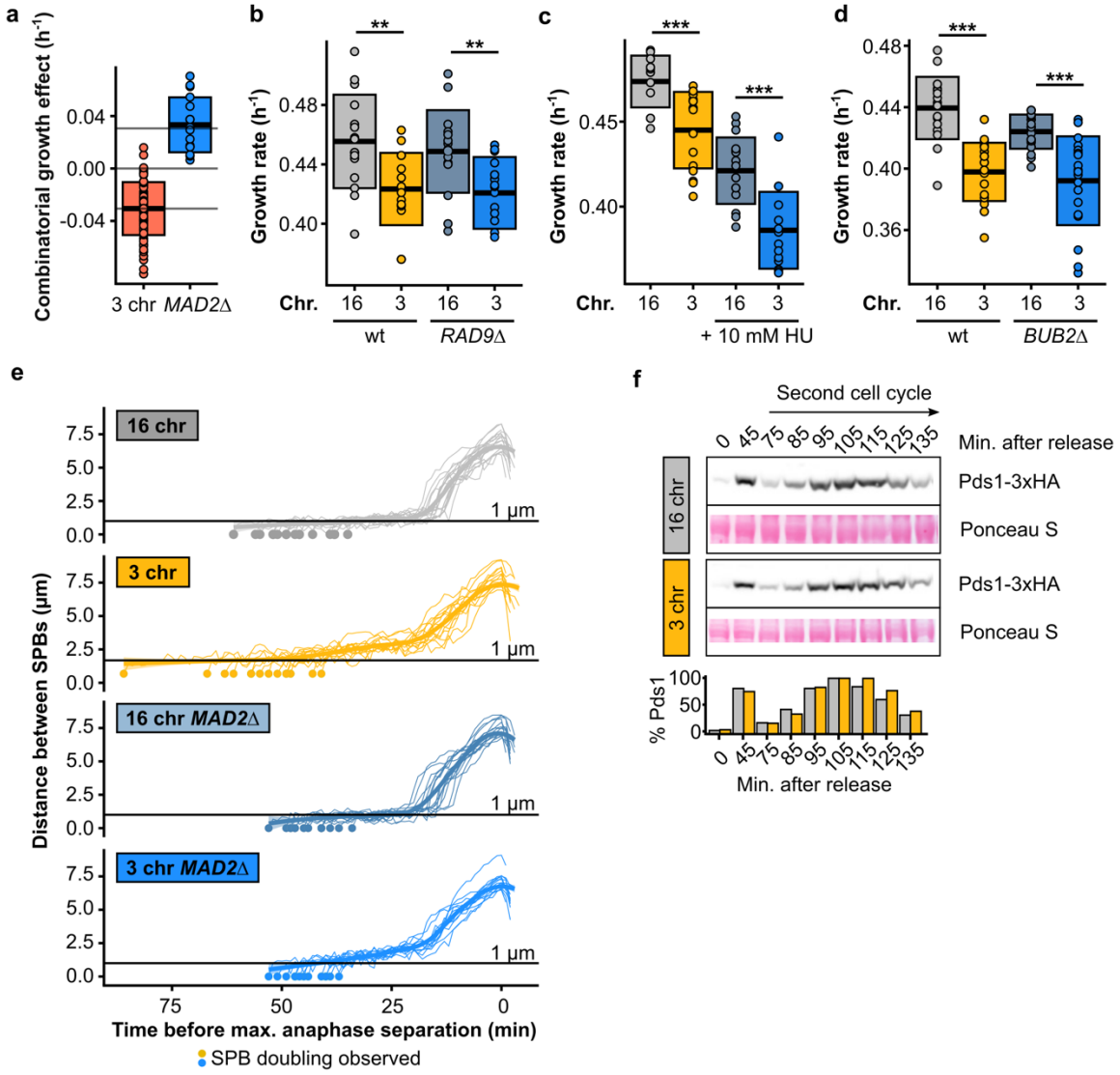

Extended Data Fig. 5 | (a) Epistatic effect of MAD2 deletion. Boxes represent means and standard deviation. **(b)** Maximum growth rates of fused-chromosome strains with and without RAD9 deletion. Boxes represent means and standard deviations. Means were compared using a Student's t-test; ** $p < 0.01$. **(c)** Maximum growth rates of fused-chromosome strains with and without 10 mM hydroxyurea. Boxes represent means and standard deviations. Means were compared using a Student's t-test; *** $p < 0.001$. **(d)** Maximum growth rates of fused-chromosome strains with and without BUB2 deletion. Boxes represent means and standard deviations. Means were compared using a Student's t-test; *** $p < 0.001$. **(e)** Distance between SPBs over time in *MAD2*Δ cells. For normalization, the time point with maximal SPB separation during anaphase was set to zero. **(f)** Western blot analysis of Pds1 levels after G1 release for 16- and 3-chromosome strains, focused on the second cell cycle after release. Cells were collected at the indicated time points. Ponceau S staining was used as a loading control. Pds1-normalised values are shown in the bar plot at the bottom.

Extended Data Table 1.
File with growth rate data. Columns represent experiment number, manuscript figure number, number of haploid chromosomes, ploidy, extra perturbation, combined genotype and growth rate (in h^{-1}).

Extended Data Table 2.
File with SPB distance data over time. Columns represent genotype, experiment number, ROI within the experiment, cell identifier (Genotype_Exp_ROI), time in raw image file, time relative to SPB doubling, time relative to max. anaphase separation, SPB distance (in µm).

Extended Data Table 3.
File with spindle curvature data. Columns represent chromosome number, image ID, spindle length (in µm), straight distance between both ends of the spindle (in µm), difference between the distances (in µm) and curvature (in %).

Extended Data Table 4.
File with growth rate data throughout evolution for 8 replicate populations. Columns represent genotype, population ID, number of generations, and growth rate (in h^{-1}).

Extended Data Table 5.
SNVs and indels found after evolution. Columns represent sample name, chromosome on which mutation was found, position of mutation, reference nucleotide sequence, alternate nucleotide sequence, allele frequency, GATK quality score, indel/SNV, systematic gene name, standard gene name, systematic gene name promoter region, standard gene name promoter region, systematic gene name 3'UTR region, standard gene name 3'UTR region, frameshift?, nonsynonymous?, reference amino acid, alternate amino acid, difference in codon usage (for synonymous mutations), and a short description of the gene's function.

Extended Data Table 6.
Quantification of kinetochore clustering. Columns represent cell identifier (Genotype_Image_ROI), genotype, SPB distance (in µm), and whether the kinetochore signal is bilobed ('y') or not ('n').

Extended Data Table 7.
Genotypes of strains used in this study.